
Article:
Leong, Z., Todd, I. orcid.org/0000-0003-0217-1658 and Goodall, R. (2018) Structural dependency of some multiple principal component alloys with the Thomas-Fermi-Dirac electron density. Scripta Materialia, 146. pp. 95-99. ISSN 1359-6462

https://doi.org/10.1016/j.scriptamat.2017.11.002

Structural dependency of some multiple principal component alloys with the Thomas-Fermi-Dirac electron density

Leong Zhaoyuan*, Iain Todd, and Russell Goodall
*zhaoyuan@sheffield.ac.uk

Department of Materials Science and Engineering, The University of Sheffield, Sir Robert Hadfield Building, Mappin Street, Sheffield, S1 3JD.

Abstract
The interplay between semi-empirical parameters for multi-principle-component alloy (or High-entropy alloy) phase prediction may be partly attributed to deviations in the Miedema mixing enthalpy from quantum principles. Thus, the electron density, $n(r_{ws})$ is investigated using a Runge-Kutta solution of the Thomas-Fermi-Dirac equation from Wigner-Seitz radius values approximated experimentally from the weighted mean volume-per-atom, following the fraction of each phase present. The results show that 1) Phase stability may be affected by alloy periodicity; and 2) A rapid drop of $n(r_{ws})$ is observed even when small amounts of the complex phase are detected, <1%), indicating the importance of understanding electronic effects.

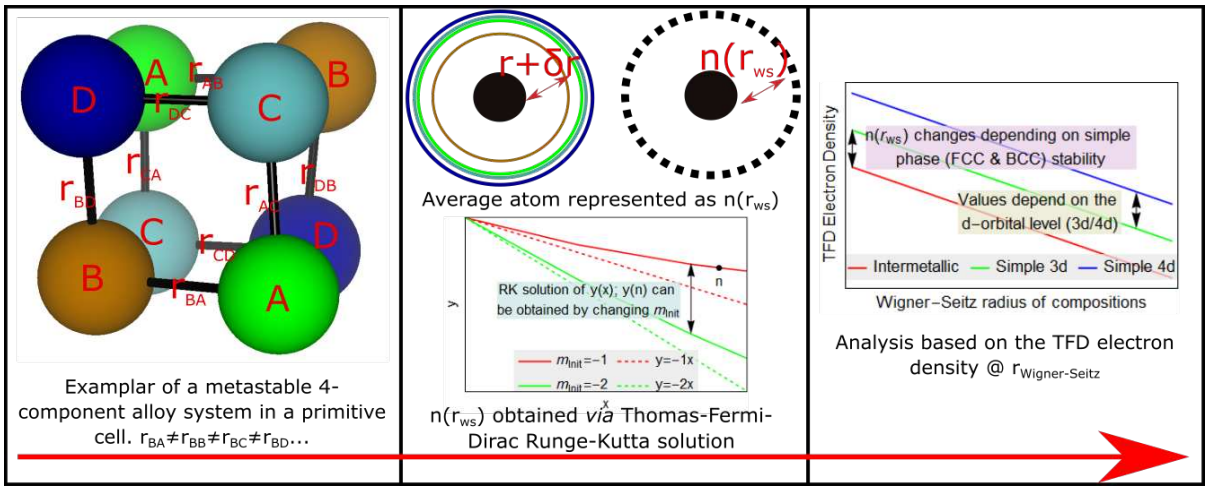

Keywords High-Entropy Alloys; XRD; Electron Density; Thomas-Fermi-Dirac; Runge-Kutta

High Entropy Alloys (HEAs) are near equimolar, multi component (>4) alloys that possess the diffraction patterns of simple phases (here defined as phases derived from the FCC, HCP, or BCC structures) [1]. These may adopt a complex phase (here defined as all non-simple phases, also known as intermetallics) [1–4]. Experiments have shown that by shifting the focus of alloy design towards the center of the phase diagram, some additional control over the phases present and some properties may be achieved, in comparison to traditional alloys where a single component dominates [5].

The synthesis and experimental characterisation of some HEA compositions, such as equimolar CoCrFeNi and CoCrFeMnNi [6] shows the existence of simple metastable structures that continue to exist at room temperature unless subjected to prolonged heat treatment [4,6], or severe plastic deformation [7]. This may reflect the near-ideal solid solution nature of simple-phase HEAs, and suggests that the solid solution formed on solidification is very nearly kinetically stabilised. Some other compositions where the CoCrFeNi composition is alloyed with some alloying addition, *A*, (here denoted as CCFN-A) are observed to destabilise the simple phase so that complex phases are observed. Examples of these compositions are additions of Ti, V, and Al to form equimolar CCFN-Ti, CCFN-V, and CCFN-Al. The presence of these complex phases suggests that the addition of Ti, V, and

Al to the CoCrFeNi composition has increased the deviation of the structure from the ideal solid solution.

Such a deviation may be predicted by calculating the enthalpy of mixing of the composition to be synthesised. For an ideal solid-solution the enthalpy of mixing is zero. In HEAs, the enthalpy of mixing is one of the terms used in some simple empirical rules for HEA alloy design [8–10] adapted from the Hume-Rothery rules of alloying [11,12]. These rules have achieved reasonable success, although accuracy is partially dependant on the composition and quantity of alloying additions [9]. The work of Dominguez *et al.* [8] uses a principal component analysis to determine two semi-empirical terms that can best describe the phase discrimination of reported HEA simple/complex phases in a 2D plot. One of these terms is the enthalpy of mixing derived from the Miedema model [13,14], and the second term is the valence electron concentration (VEC), weighted depending on the composition stoichiometry.

One critique of the Miedema model is that it has been found to be inconsistent when compared with quantum mechanical principles [15,16]. The ability of Dominguez *et al.*'s 2D plot to distinguish between components is proposed to be dependent on the deviation in the ratio between the enthalpy of mixing and the difference in the number of valence electrons squared from Miedema's model [2]. This quantity, $\Delta H / (\Delta n)^2$ has indeed been shown to diverge from theoretical predictions [16] between a VEC value of 4 to 7, which is consistent with zones of complex phase formation in HEAs [8,9]. The VEC is, in most applications of the semi-empirical rules, estimated from the weighted average of an alloy's constituents, but can only be obtained exactly using *ab-initio* calculations [2].

The difference in bonding directionality between complex structures of transition metals and simple structures in elemental metals is known [17–20]. A comparison between both shows increased structuring and localisation of electrons [20] that could indicate a reduction in the VEC of a complex phase-containing composition. Therefore, knowledge of the changes in the electronic structure could allow the analysis of such effects, to develop a more effective approach for alloy design and phase selection, and a deeper understanding of how a seemingly simply 2D plot can partition the simple and complex HEA phases. One parameter which may offer insight into this is the Wigner-Seitz radius [21–23] as it may be used to determine the cohesive properties in alloys [24], with knowledge of the valence and core electrons. One advantage is that the Wigner-Seitz radius may be approximated from experimental data of known compositions.

To look deeper into this phenomena, we therefore calculate the electron density at the Wigner-Seitz radius of several HEA compositions (as the actual VEC is connected to the electronic density) utilising the Runge-Kutta (RK) numerical solution of the Thomas-Fermi-Dirac (TFD) equation [25–27]. The TFD model is an expansion on Thomas' [28] and Fermi's [29] original work to account for the effect of electron exchange interactions to solve the many-electron problem. From the TFD Model, the electron density at absolute zero is given by:

$$n(x) = \frac{Z}{4\pi\mu^3}\left[\varepsilon + \left(\frac{\varphi(x)}{x}\right)^{1/2}\right]^3 \quad (1)$$

where $\mu = a_0\left(\frac{9\pi^2}{128Z}\right)^{1/3}$, $\varphi(x)$ is the TFD function, $n(x)$ represents the electron density, a_0 is the Bohr radius, Z is the atomic number, x is the normalised radius with $r = \mu\, x$, and $\varepsilon = \left(\frac{3}{32\pi^2}\right)^{1/3} Z^{-2/3}$ represents the electron exchange interaction term introduced by Dirac.

The second-order differential expression of the TFD equation may then be written as in Eq. (2):

$$\frac{d^2\varphi}{dx^2} = x\left[\left(\frac{\varphi(x)}{x}\right)^{1/2} + \varepsilon\right]^3 \quad (2)$$

while the associated boundary conditions in Eq. (3) & Eq. (4) for a non-isolated neutral atom which may be written as [25–27]:

$$\varphi(0) = 1 \quad (3)$$

$$\left(\frac{d\varphi}{dx}\right)_{x=x_0} = \frac{\varphi(x_0)}{x_0} \quad (4)$$

To apply the Runge-Kutta method to the TFD equation, the equation must first be expanded. A semi-convergent expansion of Eq. 2 may be written for the first 13 terms (which when evaluated in this work is sufficient to obtain at least four decimal places accuracy) as:

$$\varphi(x) = 1 + a_n(x)^{n/2} + \ldots \text{, up to n = 13} \quad (5)$$

where a_n represents the coefficients of the expansion which may be obtained by equating Eq. (5) with Eq. (2) and comparing coefficients of similar power exponents from both sides of the equation for coefficients of a_n where n = 3, 4, 5… 13, the forms of the coefficients used are listed in the supporting information and are similar to those used in previous work [25–27]. The reason that the coefficient (n = 2), a_2 is excluded is that the initial slope of the TFD equation, $\varphi'(0)$ is equated with this value, $\varphi'(0) = a_2$; allowing for any chosen value of a_2 (since the other coefficients evaluated as a function of a_2), evaluation of the expansion (Eq. 5) using the Runge-Kutta method until the boundary conditions (Eq. 3 and 4) are satisfied. Mathematically, for any value of a_2, $\varphi(x)$ approaches the x-axis asymptotically and the solution corresponds to the free atom. However, if the chosen value of a_2 is too high, r_{ws} does not match real-world values, whilst when a_2 is too steep (low) the values returned are negative which will lead to a complex solution. Based on previous work, real values of a_2 are found to lie between -1.7 to -1.5 [25,27]. By varying a_2, pairs of r_{ws} and $n(r_{ws})$ values are obtained – however, for any composition, only the pair that corresponds to the experimental r_{ws} value leads to a real $n(r_{ws})$ value. For a known crystal structure, r_{ws} may be approximated from the mean volume, *V* of the unit cell and the number of atoms of the unit cell, *N*. By assuming that each atom is spherical an average value of r_{ws} may be obtained:

$$r_{ws} = \sum_i \left(x_i \left(\frac{3V_i}{4N\pi}\right)^{1/3}\right) \quad (6)$$

where *i* is the number of phases identified for a given alloy composition, V_i is the volume of the phase *i*, and x_i is the volume fraction of phase *i*. It is useful to emphasise once more that during the attempt to solve the TFD of a given atomic number, *Z*, values of the initial gradient, a_2, each lead to unique values of both the Wigner-Seitz radius, r_{ws} and electron density, $n(r_{ws})$. Therefore, knowledge of each composition's r_{ws} is essential in determining the correct $n(r_{ws})$. Due to this and the approximation of r_{ws}, this method used here is therefore not an *ab-initio* solution of the studied compositions, but should be considered a numerical analysis probing the interactions between a change in HEA structure (as a function of volume, from which is derived r_{ws}), and its electronic structure (represented by $n(r_{ws})$). Furthermore, the method is also useful as it allows analysis as a function of the average HEA unit cell volume. Since recent research [1,5] has emphasised that a HEA may often consist of multiple simple phases, the TFD model simplifies the problem by allowing each alloy to be distinguished by only $n(r_{ws})$.

While the choice of the TFD model may not provide full information on the electronic structure of these compositions, it is useful for giving approximate results for metals [26,30]. Taking the observation that the simple structures in HEAs are commonly associated with near-ideal solid solutions [3], which may be considered to be pseudo-good-metals, and that the complex structures

may be described as semi-ordered systems (similar to intermetallics), this simple model can be used as a first step in exploring the difference in HEA simple/complex structure behaviour. Further discussion on the treatment of complex structures by the TFD and its accuracy will be discussed below.

To confirm the accuracy of the model, $n(r_{ws})$ for elemental Cu and Fe were calculated by substituting r_{ws} values obtained from atomic radii data. These values of r_{ws} correspond to 1.413Å for Cu and 1.411Å for Fe respectively, which is in agreement with experimental results [31]. Corresponding values of $n(r_{ws})$ are listed in parantheses for Cu ($2.867\times10^{29}m^{-3}$) and for Fe ($2.929\times10^{29}m^{-3}$) respectively. These values are in relatively good agreement with the previously calculated results [25,32] of Ren *et al.* [25] for Cu ($2.739\times10^{29}m^{-3}$) and Fe ($2.931\times10^{29}m^{-3}$), and are also within reasonable range of Ghosh *et al.'s* density functional approach, with Cu ($2.82\times10^{29}m^{-3}$) and Fe ($2.79\times10^{29}m^{-3}$) [23].

In this study, the lattice parameters of selected as-cast HEA compositions of type $Co_1Cr_1Fe_1Ni_1A_x$, where A = Pd, Ti, Al, and V (here denoted CCFN-A_x) from literature are used. Synthesised stoichiometries are located near the expected simple-complex transition points from each CCFN-A composition, to examine how $n(r_{ws})$ may change as the structural stability changes. The samples were synthesised by arc-melting elements of at least 99.9% purity in a water-cooled copper hearth in a backfilled Ar atmosphere. 3 mm rods were cast via suction casting into a water-cooled copper hearth under similar conditions, and the main phases present in the as-cast condition with their associated lattice parameters determined through x-ray diffraction (XRD) on a STOE-STADI diffractometer using a monochromated Mo source to avoid luminescence effects from the alloying components. Experimentally determined XRD patterns are presented in Figure 1.

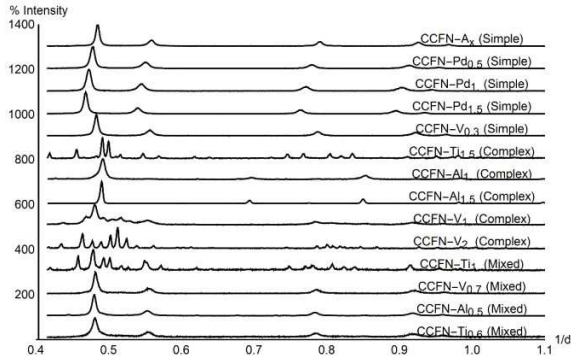

Figure 1. XRD patterns of $Co_1Cr_1Fe_1Ni_1A_x$ (denoted CCFN-A_x) where A = Al, Ti, V, Mn, and Pd with associated phase classifications as shown in Table I. The compositions CCFN-Ti, CCFN-$V_{0.7}$, CCFN-$Al_{0.5}$, and CCFN-$Ti_{0.6}$ are considered mixed compositions (containing both simple and complex phases) as low intensity peaks corresponding to a secondary phase were observed in their corresponding XRD patterns. The phases determined from the XRD patterns are tabulated and shown in Table 1; the full patterns, their peaks, phase fractions, and associated Rietveld-refined patterns and residuals may be found in the Supplementary Information.

Further addition of a fifth element to equimolar CCFN is observed to destabilise the FCC structure as the average atomic number, Z_{avg} decreases; this is the case for CCFN-Ti, CCFN-Al, and CCFN-V. Conversely, an increase in $Z_{avg,}$ as in CCFN-Pd is observed to maintain the presence of the FCC phase. The results obtained here are consistent with the predictions and observations from the literature, where complex phases are observed to be present at intermediate valence electron values [33–36]. Lattice parameters and volume fractions for the observed majority phases are obtained via Rietveld refinement (*cf.* Supplementary Information) and are used to estimate averaged r_{ws} values from Eq. (6) by weighting according to the observed volume fractions, which are listed in Table I; r_{ws} values

obtained thus are considered to be averaged values representing the electronic structure of the alloy composition. CCFN is calculated to have an r_{ws} value of 1.387 Å, and further addition of a fifth element to the composition increases r_{ws}, with CCFN-$Pd_{1.0}$ at 1.430 Å; CCFN-$Ti_{1.0}$ at 1.422 Å; CCFN-$Al_{1.0}$ at 1.418 Å; and CCFN-$V_{1.0}$ at 1.411 Å. Values for other stochiometries may be found in Table I.

The aforementioned numerical solution was programed utilising Mathematica 10.0 [37], following the steps outlined previously. The electron density at r_{ws} is then obtained for the HEA compositions mentioned previously, the full list of compositions being analysed is listed in Table I. So a meaningful comparison can be made, and to consider the effects that the base CCFN composition may have on the electronic structure, we also analyse some HEA compositions that have been reported previously. These compositions and sources may also be found in Table I.

Table I. Tabulated HEA compositions selected for this study with references where applicable, phases present (FCC/BCC/C14/Sigma/Mixed), calculated Wigner-Seitz radius (r_{ws}), and electron density obtained from the TFD model (*n(e)*). Here, a mixed phase is taken to mean the combination of a simple phase with a complex phase.

*This work

Composition	Phase/ Classification	Ref.	r_{ws} (Å)	*n(e)* ($\times 10^{29}$ m^{-3})
CCFN	FCC (Simple)	*	1.387	3.4346
CCFN-$Pd_{0.5}$	FCC (Simple)	*	1.415	3.131
CCFN-$Pd_{1.0}$	FCC (Simple)	*	1.43	3.2202
CCFN-$Pd_{1.5}$	FCC (Simple)	*	1.45	2.97
MnFeNiCo	FCC (Simple)	[8]	1.591	1.7927
$CuCrFeNi_2Mn_2$	FCC (Simple)	[38]	1.42	3.0399
$CuCr_2Fe_2Ni_2Mn_2$	FCC (Simple)	[38]	1.42	3.0042
$Cu_2CrFe_2Ni_2Mn$	FCC (Simple)	[38]	1.42	3.2107
CCFN-$V_{0.3}$	FCC (Simple)	*	1.399	3.3334
MnNbVTi	BCC (Simple)	[8]	1.546	2.1672
MoFeCrTiW	BCC (Simple)	[39]	1.54	2.2789
$AlCoCrFeNiTi_{0.5}$	BCC (Simple)	[40]	1.428	3.0242
$AlCoCrFeNiTi_{1.0}$	BCC (Simple)	[40]	1.518	2.16
MnFeNiTi	BCC (Simple)	[8]	1.516	2.1678
CCFN-$Ti_{1.5}$	C14 (Complex)	*	1.516	2.1184
CoCrFeNiCuTi	C14 (Complex)	[41]	1.413	2.9038
$AlCoCrFeNiTi_{1.5}$	C14 (Complex)	[40]	1.418	2.72
CCFN-$Al_{1.0}$	B2 (Complex)	*	1.422	2.7666
CCFN-$Al_{1.5}$	B2 (Complex)	*	1.411	2.8209
CCFN-$V_{2.0}$	Sigma (Complex)	*	1.42	2.8024
CCFN-$V_{1.0}$	Sigma (Mixed)	*	1.462	2.55
$Al_{0.5}CoCrCuFeNiTi$	Sigma (Complex)	[42]	1.406	2.8838
CCFN-Ti_1	FCC/C14 (Mixed)	*	1.407	3.1613
CCFN-$V_{0.7}$	FCC/Sigma (Mixed)	*	1.423	2.8225
CCFN-$Al_{0.5}$	FCC/B2 (Mixed)	*	1.418	2.9355
CoCrFeNiAlCu	FCC/B2(Mixed)	[43]	1.43	2.9079
CCFN-$Ti_{0.5}$	FCC/C14 (Mixed)	*	1.411	2.956
$Ta_{34}Nb_{33}Hf_8Zr_{14}Ti_{11}$	BCC (Simple 5d)	[44]	1.654	1.943
NbMoTaW	BCC (Simple 5d)	[45]	1.586	2.4797
TaNbHfZr	BCC (Simple 5d)	[46]	1.689	1.5636
VNbMoTaW	BCC (Simple 5d)	[47]	1.569	2.5759

Utilising the results of the RK solution of the TFD equation, the electron density is obtained through Eq. (1). These values are listed in Table I and are shown graphically in Figure 2 with the primary phase observed experimentally indicated. A full table containing values of the a_2 coefficient may be found in the Supplementary Information. A demarcation between HEA simple and complex phases is observed in Figure 2; with the lines in Figure 2 acting as a guide to the eye. Simple phases are further observed to be separated depending on the mean primary quantum number (which is also known as the periodicity of the elements) of the constituent alloying components (differentiated as *4d*, and *5d* in Figure 2), as the electron density scales with r_{ws} for HEAs with alloying components that are mainly from the same row of the periodic table, or have similar average primary quantum numbers due the increasing number of non-valence electrons (*c.f.* Table I). Current empirical approaches do not account for the influence of the average primary quantum number of the considered alloy, though the effect may be mirrored in new ways of depicting data.

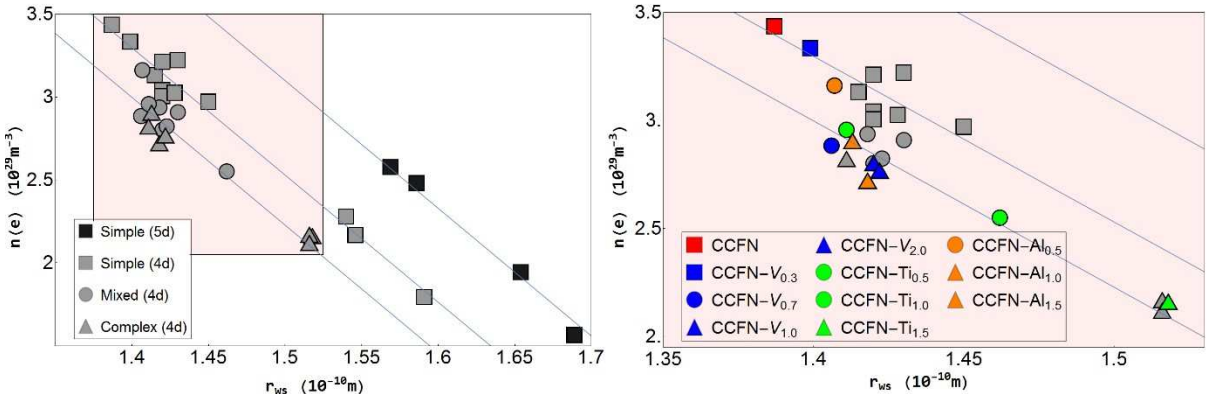

Figure 2(a). Left: Plot of calculated electron density against the Wigner-Seitz radius; showing a separation of complex and simple phases with indicator lines to guide the eye; (b) Right: Detail for CoCrFeNi-A_x alloys, or shortened to CCFN-A_x (A = V, Ti, and Al) where CCFN-V_x alloys are coloured in blue, CCFN-Ti_x alloys are coloured in green, and CCFN-Al_x alloys are coloured in orange. The plot demonstrates the effect of increasing A additions to the CCFN composition, showing a rapid lowering of the electron density, which is observed to coincide with the presence of a complex structure, even in small quantities.

The three mentioned areas shown in Figure 2(a) (indicated by the lines) each show an approximately linear relationship with r_{ws}; this may be attributed to the alloying components as over 40% of them as the alloying elements Co, Cr, Fe, and Ni feature prominently in many of the compositions. However, the demarcation between simple and complex phases is characterised by a downwards shift in the electron density for an equivalent r_{ws} value, even when the complex structures have only been detected in small quantities *via* XRD, indicating that the behaviour may not be related to segregation of the alloy. This is illustrated in the inset of Figure 2 for both CCFN-Al, CCFN-V, and CCFN-Ti HEA compositions where the occurrence of the complex phase is shown to correspond to a rapid lowering of the electron density, for both mixed (here a mixed phase is taken to mean some combination of both simple and complex phases) and complex phase compositions, indicating the influence of the alloying addition in destabilising the electronic structure of the simple phase. A rapid drop is associated with low detected amounts of the complex structure, 1.3% and 0.4% for CCFN-$V_{0.7}$ and CCFN-$Ti_{0.5}$ respectively (*cf.* Table S1). For CCFN-$Al_{0.5}$ the detected percentage of BCC/B2 was 9.5% and this higher amount may be attributed to the B2 phase being coherently present with the BCC phase in CCFN-Al_x compositions [48]; these low values are similarly observed for the CoCrFeNiAlCu composition, which possesses a FCC-B2 mixed phase.

It may be inferred from Figure 2(b), that the simple phase appears to be stabilised through alloying additions that can maintain a near-delocalised bandstructure (or good metallic-like behaviour) near the Fermi energy. The complex phases are likely to form once the addition of alloying elements with covalent-like character are able to sufficiently distort the bandstructure [19] which may occur before the precipitation of the complex structure that is detected *via* XRD; thus leading to an abrupt change in the electron density. Physically, an increase in interatomic spacing may allow for increased occupancy at interstitial sites as required, thus creating conditions for the formation of an energetically stable structure that may better reflect the state of the bandstructure. In this case, stability of HEA simple phases may possibly be achieved by maintaining the delocalisation of its electrons near its Fermi energy either through selection of non-directional alloying elements, or compensating for alloying elements that exhibit covalent-like character, which may be approximated using other HEA semi-empirical parameters such as the enthalpy of mixing. For magnetic alloys, in addition to the electronic structural effects, magnetic effects also influence and increase the complexity of the compositions [49].

In summary, we have calculated and analysed the electron densities of 14 five-component HEA compositions based on the equimolar four-component CCFN composition, together with other HEA compositions from literature. Although the results are not surprising as it is widely known that complex / intermetallic structures possess bonding features vastly different from that of metals [17–20,50–52], the key feature of this simple analysis is that it shows the effective successful structural separation between simple and complex phases within a single two-dimensional map. Current results suggest that the influence of the average primary quantum number when utilising enthalpy of mixing values may distinguish *4d*, *5d etc.* compositions in predictions for HEA alloy design. Precipitation of complex phases is also observed to be linked to a change in electronic structure behaviour which varies from that of the simple phases, showing that knowledge of both the simple and complex phase can be useful for phase predictions when combined with an appropriate method for extrapolating the Wigner-Seitz radius for multi-principal component alloys. In closing, an in-depth study of the electronic structure would be instructive in facilitating the development of an efficient alloy design strategy that accounts for all main contributions to the electronic structure for avoiding complex phase formation, as required; and to clarify the relationship between the Wigner-Seitz electron density and the formation of preferred phases.

This study is funded under the Accelerated Metallurgy FP7 European Project (FP7-NMP 263206). We would like to thank Dr. C. FREEMAN, Mr. G. ANAND and Mr. HUANG Y.h. for their helpful remarks.

References

[1] U. Dahlborg, J. Cornide, M. Calvo-Dahlborg, T.C. Hansen, A. Fitch, Z. Leong, S. Chambreland, R. Goodall, Structure of some CoCrFeNi and CoCrFeNiPd multicomponent HEA alloys by diffraction techniques, J. Alloys Compd. 681 (2016) 330–341. doi:10.1016/j.jallcom.2016.04.248.

[2] Z. Leong, J.S. Wróbel, S.L. Dudarev, R. Goodall, I. Todd, D. Nguyen-Manh, The Effect of Electronic Structure on the Phases Present in High Entropy Alloys, Sci. Rep. 7 (2017) 39803. doi:10.1038/srep39803.

[3] F. Otto, Y. Yang, H. Bei, E.P. George, Relative effects of enthalpy and entropy on the phase stability of equiatomic high-entropy alloys, Acta Mater. 61 (2013) 2628–2638. doi:10.1016/j.actamat.2013.01.042.

[4] F. Otto, A. Dlouhý, K.G. Pradeep, M. Kuběnová, D. Raabe, G. Eggeler, E.P. George, Decomposition of the single-phase high-entropy alloy CrMnFeCoNi after prolonged anneals at intermediate temperatures, Acta Mater. 112 (2016) 40–52. doi:10.1016/j.actamat.2016.04.005.

[5] D.B. Miracle, O.N. Senkov, A critical review of high entropy alloys and related concepts, Acta Mater. 122 (2017) 448–511. doi:10.1016/j.actamat.2016.08.081.

[6] E.J. Pickering, R. Munoz-Moreno, H.J. Stone, N.G. Jones, Precipitation in the equiatomic high-entropy alloy CrMnFeCoNi, Scr. Mater. 113 (2016).

[7] B. Schuh, F. Mendez-Martin, B. Völker, E.P. George, H. Clemens, R. Pippan, A. Hohenwarter, Mechanical properties, microstructure and thermal stability of a nanocrystalline CoCrFeMnNi high-entropy alloy after severe plastic deformation, Acta Mater. 96 (2015) 258–268. doi:10.1016/j.actamat.2015.06.025.

[8] L.A. Dominguez, R. Goodall, I. Todd, Prediction and validation of quaternary high entropy alloys using statistical approaches, Mater. Sci. Technol. 31 (2015) 1201–1206.

[9] S. Guo, N. C, L. J, L.C. T, Effect of valence electron concentration on stability of fcc or bcc phase in high entropy alloys, J. Appl. Phys. 109 (2011) 10.

[10] Y. Zhang, X. Yang, P.K. Liaw, Alloy design and properties optimisation of high-entropy alloys, J. Mater. Miner. Min. Soc. 64 (2012) 830–838.

[11] A. Paxton, M. Methfessel, D.G. Pettifor, A bandstructure view of the Hume-Rothery electron phases, Proc. R. Soc. A. 453 (1997) 1493.

[12] W. Hume-Rothery, R.E. Smallman, C.W. Haworth, The Structure of Metals and Alloys, The Institute of Metals, Carlton House Terrace, London SW1Y 5DB, UK, 1988.

[13] A.R. Miedema, The electronegativity parameter for transition metals: Heat of formation and charge transfer in alloys, J. Common Met. 32 (1973) 117–136. doi:10.1016/0022-5088(73)90078-7.

[14] H. Bakker, A. Miedema, Enthalpies in alloys: Miedemaś semi-empirical model, Trans Tech Publications, Uetikon-Zuerich, Switzerland ; Enfield, N.H, 1998.

[15] D.G. Pettifor, A Quantum Mechanical Critique of the Miedema Rules for Alloy Formation, Solid State Phys. 40 (1987) 43–92.

[16] D.G. Pettifor, Theory of the Heats of Formation of Transition-Metal Alloys, Phys. Rev. Lett. 42 (1978) 846.

[17] D.G. Pettifor, Theoretical predictions of structure and related properties of intermetallics, Mater. Sci. Technol. 8 (1992) 345–349. doi:10.1179/mst.1992.8.4.345.

[18] D.G. Pettifor, Structure Maps for Ordered Intermetallics, in: C.T. Liu, R.W. Cahn, G. Sauthoff (Eds.), Ordered Intermet. — Phys. Metall. Mech. Behav., Springer Netherlands, Dordrecht, 1992: pp. 47–59. http://link.springer.com/10.1007/978-94-011-2534-5_4 (accessed April 27, 2016).

[19] M.E. Eberhart, The metallic bond: Elastic properties, Acta Mater. 44 (1996) 2495–2504. doi:10.1016/1359-6454(95)00347-9.

[20] B. Silvi, C. Gatti, Direct Space Representation of the Metallic Bond, J. Phys. Chem. A. 104 (2000) 947–953. doi:10.1021/jp992784c.

[21] C.H. Hodges, Interpretation of the alloying tendencies of nontransition metals, J. Phys. F Met. Phys. 7 (1977) L247–L254. doi:10.1088/0305-4608/7/9/002.
[22] J.A. Alonso, L.A. Girifalco, Nonlocality and the energy of alloy formation, J. Phys. F Met. Phys. 8 (1978) 2455–2460. doi:10.1088/0305-4608/8/12/007.
[23] A.K. Ghosh, S. Chakraborty, A. Manna, Density Functional Approach for Metals. The Matheiss Prescription, Phys. Status Solidi B. 118 (1983) 373–379. doi:10.1002/pssb.2221180143.
[24] Y. Tal, Cohesive properties of metals as determined from atomic charge densities, Can. J. Chem. 74 (1996) 870–874. doi:10.1139/v96-095.
[25] F. Ren, K. Cao, J. Ren, A.A. Volinsky, T.H. Tran, B. Tian, Numerical Calculation of the Electron Density at the Wigner–Seitz Radius Based on the Thomas–Fermi–Dirac Equation, J. Comput. Theor. Nanosci. 11 (2014) 344–347. doi:10.1166/jctn.2014.3358.
[26] R.P. Feynman, N. Metropolis, E. Teller, Equations of State of Elements Based on the Generalized Fermi-Thomas Theory, Phys. Rev. 75 (1949) 1561–1573. doi:10.1103/PhysRev.75.1561.
[27] N. Metropolis, J.R. Reitz, Solutions of the Fermi-Thomas-Dirac Equation, J. Chem. Phys. 19 (1951) 555. doi:10.1063/1.1748292.
[28] L.H. Thomas, The calculation of atomic fields, Math. Proc. Camb. Philos. Soc. 23 (1927) 542. doi:10.1017/S0305004100011683.
[29] E. Fermi, Un metodo statistico per la determinazione di alcune priorieta dell'atome, Rend Accad Naz Lincei. 6 (1927) 32.
[30] J.C. Slater, H.M. Krutter, The Thomas-Fermi Method for Metals, Phys. Rev. 47 (1935) 559–568. doi:10.1103/PhysRev.47.559.
[31] P. Politzer, R.G. Parr, D.R. Murphy, Approximate determination of Wigner-Seitz radii from free-atom wave functions, Phys. Rev. B. 31 (1985) 6809–6810. doi:10.1103/PhysRevB.31.6809.
[32] C. Ke, Calculation of the Electron Density on the Surface of Atoms and Research of Internal Stress in Films Based on Cheng's Theory, Henan University of Science and Technology, 2011.
[33] G.A. Salishchev, M.A. Tikhonovsky, D.G. Shaysultanov, N.D. Stepanov, A.V. Kuznetsov, I.V. Kolodiy, A.S. Tortika, O.N. Senkov, Effect of Mn and V on structure and mechanical properties of high-entropy alloys based on CoCrFeNi system, J. Alloys Compd. 591 (2014) 11–21. doi:10.1016/j.jallcom.2013.12.210.
[34] N.D. Stepanov, D.G. Shaysultanov, G.A. Salishchev, M.A. Tikhonovsky, E.E. Oleynik, A.S. Tortika, O.N. Senkov, Effect of V content on microstructure and mechanical properties of the CoCrFeMnNiVx high entropy alloys, J. Alloys Compd. 628 (2015) 170–185. doi:10.1016/j.jallcom.2014.12.157.
[35] H.P. Chou, Y.S. Chang, S.K. Chen, J.W. Yeh, Microstructure, thermophysical and electrical properties in Al x CoCrFeNi ($0 \leq x \leq 2$) high-entropy alloys, Mater. Sci. Eng. B. 163 (2009) 184–189.
[36] T.T. Shun, L.Y. Chang, M.H. Shiu, Microstructures and mechanical properties of multiprincipal component CoCrFeNiTix alloys, Mater. Sci. Eng. A. 556 (2012) 170–174.
[37] W. Research, Mathematica 10.4, 10.4, Champaign, Illinios, 2016.
[38] B. Ren, Z.X. Liu, B. Cai, M.X. Wang, L. Shi, Aging behavior of a CuCr2Fe2NiMn high-entropy alloy, Mater. Des. 33 (2012) 121–126. doi:10.1016/j.matdes.2011.07.005.
[39] B. Zheng, Q.B. Liu, L.Y. Zhang, Microstructure and Properties of MoFeCrTiW High-Entropy Alloy Coating Prepared by Laser Cladding, Adv. Mater. Res. 820 (2013) 63–66. doi:10.4028/www.scientific.net/AMR.820.63.
[40] Y.J. Zhou, Y. Zhang, Y.L. Wang, G.L. Chen, Solid solution alloys of AlCoCrFeNiTi x with excellent room-temperature mechanical properties, Appl. Phys. Lett. 90 (2007) 181904. doi:10.1063/1.2734517.
[41] X.F. Wang, Y. Zhang, Y. Qiao, G.L. Chen, Novel microstructure and properties of multicomponent CoCrCuFeNiTix alloys, Intermetallics. 15 (2007) 357–362. doi:10.1016/j.intermet.2006.08.005.

[42] M.-R. Chen, S.-J. Lin, J.-W. Yeh, S.-K. Chen, Y.-S. Huang, C.-P. Tu, Microstructure and Properties of Al0.5CoCrCuFeNiTix (x=0–2.0) High-Entropy Alloys, Mater. Trans. 47 (2006) 1395–1401. doi:10.2320/matertrans.47.1395.
[43] L. Xie, P. Brault, A.-L. Thomann, J.-M. Bauchire, AlCoCrCuFeNi high entropy alloy cluster growth and annealing on silicon: A classical molecular dynamics simulation study, Appl. Surf. Sci. 285 (2013) 810–816. doi:10.1016/j.apsusc.2013.08.133.
[44] P. Koželj, S. Vrtnik, A. Jelen, S. Jazbec, Z. Jagličić, S. Maiti, M. Feuerbacher, W. Steurer, J. Dolinšek, Discovery of a Superconducting High-Entropy Alloy, Phys. Rev. Lett. 113 (2014). doi:10.1103/PhysRevLett.113.107001.
[45] Y. Zou, S. Maiti, W. Steurer, R. Spolenak, Size-dependent plasticity in an Nb25Mo25Ta25W25 refractory high-entropy alloy, Acta Mater. 65 (2014) 85–97. doi:10.1016/j.actamat.2013.11.049.
[46] S. Maiti, W. Steurer, Structural-disorder and its effect on mechanical properties in single-phase TaNbHfZr high-entropy alloy, Acta Mater. 106 (2016) 87–97. doi:10.1016/j.actamat.2016.01.018.
[47] O.N. Senkov, G.B. Wilks, J.M. Scott, D.B. Miracle, Mechanical properties of Nb25Mo25Ta25W25 and V20Nb20Mo20Ta20W20 refractory high entropy alloys, Intermetallics. 19 (2011) 698–706. doi:10.1016/j.intermet.2011.01.004.
[48] Y. Ma, B. Jiang, C. Li, Q. Wang, C. Dong, P. Liaw, F. Xu, L. Sun, The BCC/B2 Morphologies in AlxNiCoFeCr High-Entropy Alloys, Metals. 7 (2017) 57. doi:10.3390/met7020057.
[49] M. Calvo-Dahlborg, J. Cornide, Tobola, D. Nguyen Manh, J.S. Wróbel, J. Juraszek, S. Jouen, U. Dahlborg, Effect of Pd on structural and magnetic properties of high entropy CoCrFeNiPd alloys. In preparation, (2016).
[50] N.E. Christensen, Structural phase stability of B2 and B32 intermetallic compounds, Phys. Rev. B. 32 (1985) 207–228. doi:10.1103/PhysRevB.32.207.
[51] G.A. Botton, G.Y. Guo, W.M. Temmerman, C.J. Humphreys, Experimental and theoretical study of the electronic structure of Fe, Co, and Ni aluminides with the *B* 2 structure, Phys. Rev. B. 54 (1996) 1682–1691. doi:10.1103/PhysRevB.54.1682.
[52] Y. Sumitomo, T. Moriya, H. Ino, F. Eiichi Fujita, The Mossbauer Effect of Fe-V and Fe-Cr Sigma Phase, J. Phys. Soc. Jpn. 35 (1973) 461–468. doi:10.1143/JPSJ.35.461.